Rising Temperatures Increase Importance of Oceanic Evaporation as a Source for Continental Precipitation

KIRSTEN L. FINDELL,[a] PATRICK W. KEYS,[b] RUUD J. VAN DER ENT,[c,d] BENJAMIN R. LINTNER,[e] ALEXIS BERG,[f] AND JOHN P. KRASTING[a]

[a] *NOAA/Geophysical Fluid Dynamics Laboratory, Princeton, New Jersey*
[b] *School of Global Environmental Sustainability, Colorado State University, Fort Collins, Colorado*
[c] *Department of Water Management, Faculty of Civil Engineering and Geosciences, Delft University of Technology, Delft, Netherlands*
[d] *Department of Physical Geography, Faculty of Geosciences, Utrecht University, Utrecht, Netherlands*
[e] *Department of Environmental Sciences, Rutgers, The State University of New Jersey, New Brunswick, New Jersey*
[f] *Department of Civil and Environmental Engineering, Princeton University, Princeton, New Jersey*

(Manuscript received 26 February 2019, in final form 12 August 2019)

ABSTRACT

Understanding vulnerabilities of continental precipitation to changing climatic conditions is of critical importance to society at large. Terrestrial precipitation is fed by moisture originating as evaporation from oceans and from recycling of water evaporated from continental sources. In this study, continental precipitation and evaporation recycling processes in the Earth system model GFDL-ESM2G are shown to be consistent with estimates from two different reanalysis products. The GFDL-ESM2G simulations of historical and future climate also show that values of continental moisture recycling ratios were systematically higher in the past and will be lower in the future. Global mean recycling ratios decrease 2%–3% with each degree of temperature increase, indicating the increased importance of oceanic evaporation for continental precipitation. Theoretical arguments for recycling changes stem from increasing atmospheric temperatures and evaporative demand that drive increases in evaporation over oceans that are more rapid than those over land as a result of terrestrial soil moisture limitations. Simulated recycling changes are demonstrated to be consistent with these theoretical arguments. A simple prototype describing this theory effectively captures the zonal mean behavior of GFDL-ESM2G. Implications of such behavior are particularly serious in rain-fed agricultural regions where crop yields will become increasingly soil moisture limited.

1. Motivation

Human populations and terrestrial ecosystems throughout the world depend on precipitation as a primary water source, particularly in water-limited regions. Understanding the spatial distribution of the moisture sources for terrestrial precipitation can expose regional vulnerabilities to changes in evaporation in upwind source areas (Keys et al. 2012). Upwind oceanic evaporation contributing to regional precipitation is largely determined by ocean circulation patterns, as well as external factors and climate feedbacks that drive sea surface temperatures (e.g., solar radiation, aerosols, and greenhouse gases; Soden and Held 2006). Upwind terrestrial evaporation, however, is dependent on both climatic factors and land surface conditions such as vegetation and soil moisture conditions. Many studies have investigated hydrologic connections between source and sink areas from a regional perspective (e.g., Bosilovich and Chern 2006; Dirmeyer and Brubaker 2007; Dominguez et al. 2006) or from a global perspective (e.g., Koster et al. 1986; Trenberth 1999; Bosilovich et al. 2005). This study is, to our knowledge, the first to focus on how historical and projected climate change affects the relative contributions of oceanic and terrestrial moisture to continental precipitation. This research sheds light on the global hydrological cycle and how it will change in a warming world; as such, it speaks directly to the science

Supplemental information related to this paper is available at the Journals Online website: https://doi.org/10.1175/JCLI-D-19-0145.s1.

Corresponding author: Kirsten L. Findell, kirsten.findell@noaa.gov

DOI: 10.1175/JCLI-D-19-0145.1

questions posed by the Global Energy and Water Exchanges (GEWEX) project of the World Climate Research Program.

In the next section we introduce the Earth system model GFDL-ESM2G (hereinafter ESM2G; acronym definitions can be found at https://www.ametsoc.org/PubsAcronymList) and the reanalysis datasets used to confront the model, and we describe the water tracking algorithm known as the Water Accounting Model—2 layers (WAM-2layers; van der Ent et al. 2014). In section 3 we present moisture tracking results from the three datasets described in section 2, and in section 4 we show additional results from the model's past and future simulations. Section 5 provides a synthesis of current understanding of how the hydrologic cycle will change in a warming climate. This understanding is used to generate a simple prototype model of continental moisture recycling in a changing climate. We then explore how soil moisture limitations influence these processes. Discussion and conclusions are presented in the final section.

2. Datasets and methods

a. Model description: ESM2G

ESM2G (Dunne et al. 2012, 2013) is a fully coupled numerical Earth system model developed by NOAA's Geophysical Fluid Dynamics Laboratory (GFDL). ESM2G simulates physical interactions among different components of the Earth system and includes a coupled simulation of the carbon cycle. The atmosphere and land components of ESM2G have a horizontal resolution of approximately 2°, and the ocean and sea ice components have a resolution of approximately 1°. ESM2G uses the same atmosphere component (AM2; Anderson et al. 2004) as the GFDL CM2.1 (Delworth et al. 2006) coupled climate model with 24 vertical levels. Simulation of the physical ocean is performed using the Generalized Ocean Layer Dynamics model (GOLD; Hallberg and Adcroft 2009), which uses a 63-layer isopycnal vertical coordinate and is coupled to the Tracers of Phytoplankton and Allometric Zooplankton (TOPAZ) biogeochemistry model. The land component of the model (LM3; Shevliakova et al. 2009) simulates both hydrology and dynamic terrestrial vegetation. Sea ice is simulated using the GFDL Sea Ice Simulator (SIS), version 1 (Winton 2000). Further documentation of the physical climate and carbon cycle simulations is presented in two papers by Dunne et al. (2012, 2013).

We analyze results from simulations performed as part of phase 5 of the Coupled Model Intercomparison Project (CMIP5; Taylor et al. 2012), but with additional subdaily output saved to meet the requirements of the WAM-2layers water tracking algorithm, as described below. The preindustrial control simulation ("piControl") is integrated for 500 yr with persistent fixed forcing (i.e., year 1860) from well-mixed greenhouse gases, aerosols, solar radiation, and volcanoes. The "historical" simulations (years 1861–2005) include time-varying histories of these climate forcings along with historical reconstructions of land use change. The future climate scenarios (years 2006–2100) are based on the IPCC representative concentration pathway scenario RCP8.5, where atmospheric CO_2 increases to 1370 ppmv by the year 2100. Three ensemble members, each starting at 100-yr intervals from the piControl simulation, are performed for the historical and "RCP8.5" simulations to represent internal climate variability from the model.

b. Dataset descriptions: MERRA and ERA-Interim reanalyses

We use the ERA-Interim reanalysis data produced by the European Centre for Medium-Range Weather Forecasts (Dee et al. 2011), and the Modern-Era Retrospective Analysis for Research and Applications (MERRA) reanalysis produced by the National Aeronautics and Space Administration (Bosilovich et al. 2011). We use ERA-Interim at the $1.5° \times 1.5°$ resolution from the years 1979 to 2014, and MERRA data at the $1.0° \times 1.25°$ resolution from the years 1979 to 2012. Both ERA-Interim and MERRA reproduce precipitation reasonably well over land (e.g., Trenberth et al. 2011), but ERA-Interim tends to overestimate precipitation in some high-altitude regions (e.g., the Andes and the Tibetan Plateau), as well as parts of the Congo River basin (Lorenz and Kunstmann 2012). MERRA, conversely, overestimates precipitation in parts of central South America (Dirmeyer et al. 2014). Despite these differences, a previous moisture recycling comparison of ERA-Interim and MERRA demonstrated consistency between these reanalyses, particularly in matching key sources and sinks of atmospheric moisture across multiple continents (Keys et al. 2014).

c. Water tracking algorithm description: WAM-2layers

We apply the water tracking algorithm WAM-2layers (van der Ent et al. 2010, 2014) to track continental evaporation E forward in time and continental precipitation P backward in time in separate tracking experiments. The tracking algorithm is offline and is configured to use output of MERRA, ERA-Interim, and ESM2G. The data used are 3-hourly inputs of surface evaporation and precipitation, and 6-hourly inputs

of surface pressure and the pressure-level fields of zonal and meridional wind speeds and specific humidity. These data are used to solve the water balance of tagged moisture (subscript g) in an upper and lower layer, $S_{g,\text{upper}}$ and $S_{g,\text{lower}}$, where S is moisture in the atmospheric column. These calculations do not influence the total water balance. In forward tracking mode the water balance of tagged moisture in the lower layer is given by

$$\frac{\partial S_{g,\text{lower}}}{\partial t} = -\frac{\partial (S_{g,\text{lower}} u)}{\partial x} - \frac{\partial (S_{g,\text{lower}} v)}{\partial y} + E_g - P_g \pm F_{v,g},$$

where F_v is vertical exchange between the layers. Equations for the upper layer and backward tracking are similar. The fluxes $\partial(S_{g,\text{lower}}u)/\partial x$ and $\partial(S_{g,\text{lower}}v)/\partial y$ are calculated over gridcell boundaries in an explicit forward scheme. Note that E_g is considered always to enter the lower layer only. For these experiments, tracking continental moisture E_g is equal to E over land areas and 0 over oceanic grid cells. The tracked moisture store is depleted by precipitation assuming that $P_g/P = S_g/S$. The vertical exchange F_v with the upper layer is parameterized to minimize water balance losses in the combined upper and lower store. The gross vertical flow is 4 times the vertical flow in the net flow direction and 3 times the vertical flow in the opposite direction. The distinction between the gross and net vertical exchange flow is to account for the fact that most of the water vapor exchange between the lower and upper parts of the atmosphere happens in processes that lead to more mixing than we would assume based on simple upward or downward large-scale advective flow. This exchange is intended to capture all exchanges due to convection, turbulence, and rainfall that does not reach the surface because of re-evaporation and other processes. Although the vertical exchange is a strong assumption in WAM-2layers, physically reasonable results have been obtained (van der Ent et al. 2014). The general tracking in two layers has also been validated against an online 3D tracking method and similar results were obtained (van der Ent et al. 2013). The time step of the tracking for all methods was set to 15 min for computational stability.

Minor numerical losses of water arise from temporal interpolation of WAM-2layers input fields from 3- or 6-hourly data down to 15-min increments, from the vertical interpolation of full atmospheric profiles of wind and humidity down to two layers, and from the neglect of frozen and liquid water in the atmosphere (i.e., only water vapor is tracked). These losses lead to an imperfect balance between the forward tracking of continental evaporation until it precipitates out over land (E_c), and the backward tracking of continental precipitation to its source as land-based evaporation (P_c). In the annual mean, these terms should be identical. We apply a correction procedure to account for loss terms and ensure that $P_{c\_\text{corr}} = E_{c\_\text{corr}}$. This correction procedure is described in the appendix. All terms henceforth refer to the corrected values.

Tracking moisture directly within the full GCMs or reanalyses would provide a more accurate accounting of moisture and avoid the need for the procedure detailed in the appendix to ensure consistency between the forward-tracking and backward-tracking results. However, this is a computationally expensive proposition that is not currently implemented at any modeling centers that we are aware of. WAM-2layers provides a consistent method to investigate moisture transport on model and reanalysis output.

3. Continental moisture tracking in model and reanalysis datasets

The schematic shown in Fig. 1 depicts the continental precipitation and evaporation recycling ratios—ρ_c and ε_c, respectively—introduced by van der Ent et al. (2010). The continental precipitation recycling ratio quantifies the dependence of terrestrial precipitation on moisture previously evaporated from terrestrial source regions, and is defined as

$$\rho_c(t,x,y) = \frac{P_c(t,x,y)}{P_c(t,x,y) + P_o(t,x,y)} = \frac{P_c(t,x,y)}{P_{\text{Land}}(t,x,y)}, \quad (1)$$

where P_{Land} is total continental precipitation and P_c and P_o are the backward-tracked portions of this precipitation originating from continental and oceanic sources, respectively. Similarly, the continental evaporation recycling ratio ε_c is a measure of the fraction of terrestrial evaporation that ultimately precipitates back onto land:

$$\varepsilon_c(t,x,y) = \frac{E_c(t,x,y)}{E_c(t,x,y) + E_o(t,x,y)} = \frac{E_c(t,x,y)}{E_{\text{Land}}(t,x,y)}, \quad (2)$$

where E_{Land} is total continental evaporation, E_c is terrestrial evaporation tracked forward until it precipitates out over land, and E_o is the remainder of terrestrial evaporation that eventually precipitates out over the ocean. These terms are shown in the Fig. 1 schematic for the global-scale case in which $E_c = P_c$. The moisture flux values in this figure will be discussed in section 4 below.

Figure 2 depicts global maps of the fraction of local precipitation that last evaporated from land (Figs. 2b,d,f) and the fraction of local evaporation that precipitates out over land (Figs. 2a,c,e) calculated using the water

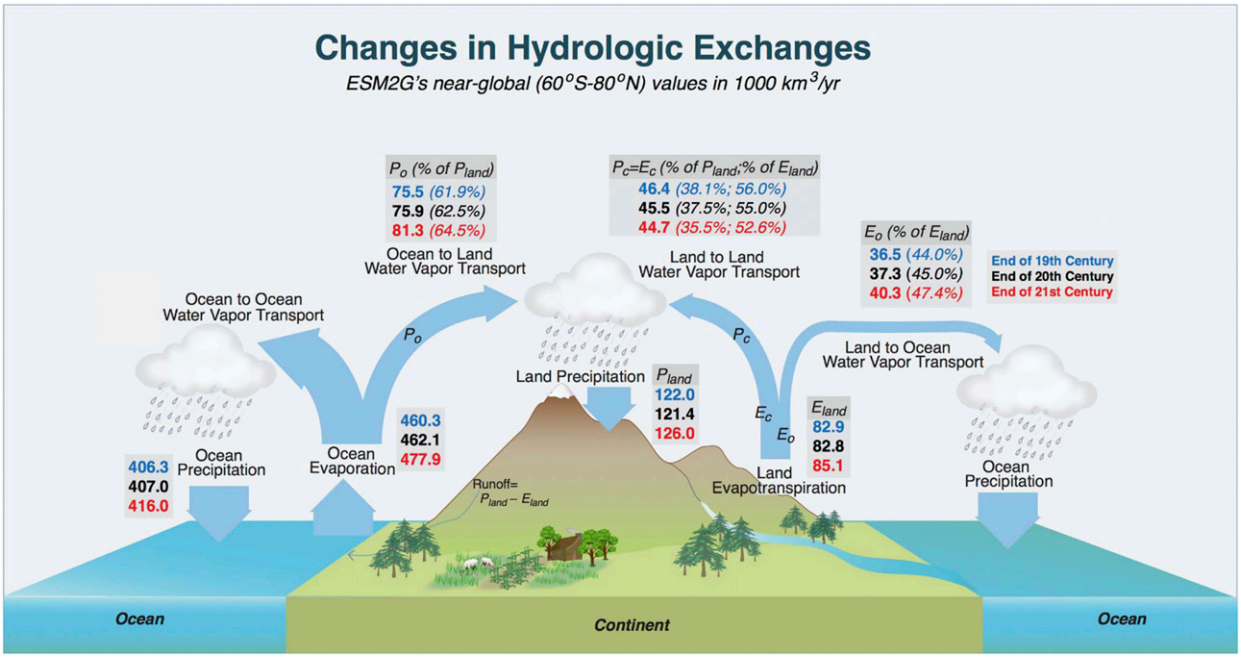

FIG. 1. Schematic depiction of continental-scale hydrologic exchanges in ESM2G for the three time periods of study: end of nineteenth century (blue), end of twentieth century (black), and end of twenty-first century (red). Boldface values are in 1000 $km^3\ yr^{-1}$. The percentages demonstrate that oceanic terms P_o and E_o are growing in relative importance in a warming world, whereas continental moisture recycling terms P_c and E_c and continental moisture recycling ratios $\rho_c = P_c/P_{\text{Land}}$ and $\varepsilon_c = E_c/E_{\text{Land}}$ are shrinking in relative importance as global temperatures warm. The values shown are for near-global (60°S–80°N) accounting; some water vapor is transported out of the domain toward high-latitude regions where precipitation typically exceeds evaporation.

tracking algorithm WAM-2layers described above (van der Ent et al. 2014) and corrected to ensure consistency between the forward- and backward-tracking routines (see the appendix) applied to the two reanalysis data products, ERA-Interim and MERRA, and to ESM2G. Over land, these mapped quantities are the ρ_c and ε_c terms defined in Eqs. (1) and (2) above. The quantities are shown over both land and ocean in Fig. 2 to better compare global moisture transport between the model and the reanalyses.

Near-global (60°S–80°N) average values of the continental moisture recycling ratios during the late twentieth (and early twenty-first) century from reanalyses and the late nineteenth, twentieth, and twenty-first centuries from the ESM2G simulations are given in Table 1. The spatial patterns of both ratios bear the imprint of prevailing circulation patterns and continental geometry (Fig. 2). For example, low precipitation recycling values (~0.1–0.3) occur along upwind coastal margins such as the west coast of North America, whereas high ρ_c values (~0.7–0.9) are seen in downwind continental regions such as the eastern half of Asia. Similarly, low evaporation recycling ratios are seen along the eastern margins of North America and Asia since evaporation from these land surfaces is typically advected out to the oceans before it can precipitate again, whereas high ε_c values are evident in upwind continental interiors. Figure 2 and Table 1 indicate that ESM2G broadly captures spatial signatures of continental ρ_c and ε_c that are similar to those for the recently observed time period in the ERA-Interim and MERRA reanalyses, albeit with better model correspondence to the former for ρ_c and to the latter for ε_c.

For broad spatial regions and annual time scales such as those considered here, water balance constraints require that $P_{\text{Land}} = E_{\text{Land}} + R_{\text{Land}}$, where R_{Land} is total continental runoff. (We assume that long-term changes in soil moisture are small relative to the other terms.) Considering the entire global land surface at these time scales, the forward and backward tracking of all continental moisture must yield identical volumes of tracked water; that is, the amount of precipitation on land originating from continental evaporation must equal the amount of continental evaporation that eventually precipitates out over land, or $P_c = E_c$, as depicted in Fig. 1. Given that $R_{\text{Land}} > 0$, water balance implies that $E_{\text{Land}} < P_{\text{Land}}$. Equations (1) and (2) then yield $\varepsilon_c > \rho_c$. All results in Table 1 obey this water balance constraint, with ε_c values exceeding the ρ_c values by 0.125–0.179.

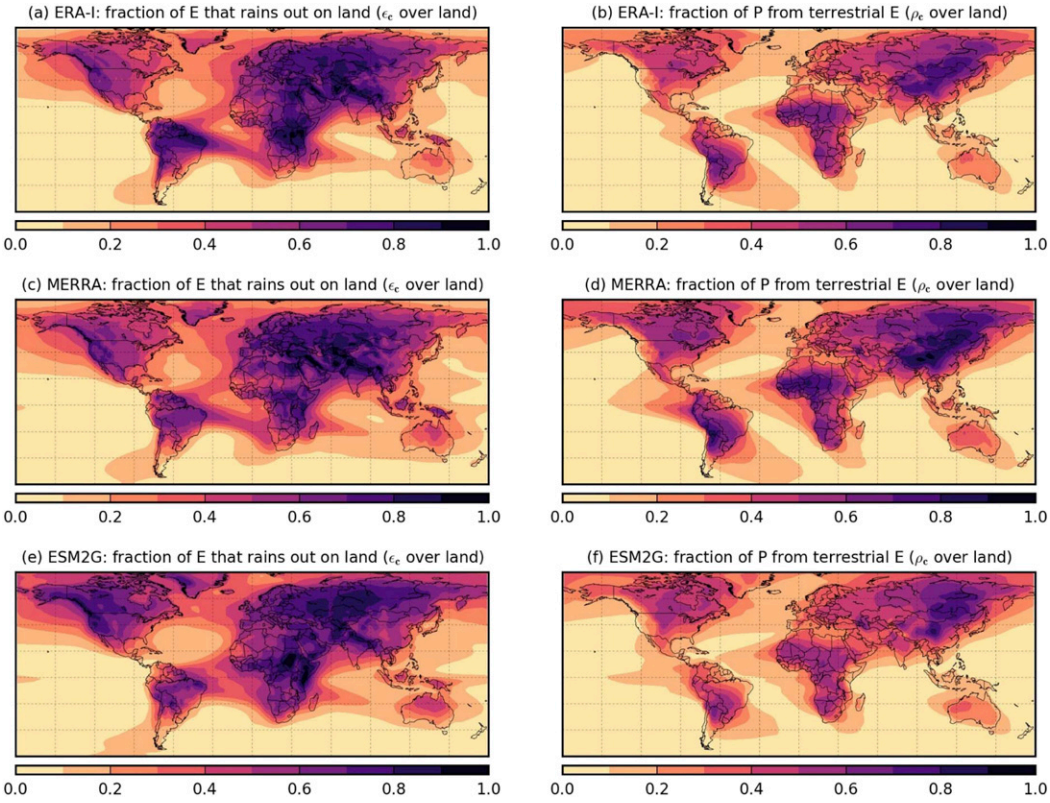

FIG. 2. The (left) fraction of local evaporation that precipitates out over land and (right) fraction of local precipitation that last evaporated from land. Over land pixels, these are continental evaporation (left column) and precipitation (right column) recycling ratios for (a),(b) ERA-Interim, (c),(d) MERRA, and (e),(f) ESM2G. ERA-Interim data cover 1979–2014. MERRA spans 1979–2012. ESM2G results are averaged over 1981–2005 from three ensemble members of historical simulations.

4. Continental moisture recycling in a warming world

Changes in continental recycling during a period of increasing atmospheric greenhouse gas concentrations and global surface temperatures are assessed using ESM2G simulations from the late nineteenth through the late twenty-first centuries. A comparison of ESM2G's computed values of late-twentieth-century ε_c and ρ_c with the 1870s-era and 2090s-era values indicates that the recycling ratios trend toward consistently smaller values from the 1870s through the end of the twenty-first century (Figs. 1 and 3, Table 1). Although the magnitude of the changes is small, with zonal mean differences of ~2%–8% in the future (red lines in Figs. 3f and 3h), the changes in Figs. 3a–d are systematic across all landmasses with a few regional exceptions (e.g., West Africa and the Iberian Peninsula). For the zonal means (Figs. 3e–h), the differences between the ends of the twentieth and twenty-first centuries are statistically different from zero at almost all latitudes. Averaged over most of the globe (60°S–80°N), Fig. 1 shows that oceanic terms P_o and E_o are growing in relative importance in a warming world, while continental moisture recycling terms P_c and E_c are shrinking in relative importance as global temperatures warm. The incremental decreases in both continental moisture recycling ratios ε_c and ρ_c indicate that, from the end of the nineteenth century to the end of the twentieth century, the importance of oceanic sources for continental hydrology increases by 1.6%–1.8%, with a further increase of 4.4%–5.3% projected by the end of the twenty-first century (Table 1). Scaling the recycling changes by the simulated global mean warming of 0.56°C between the first two time periods yields a sensitivity of about 3% per degree of global warming; between the latter two time periods, with 2.65°C of warming, the sensitivity is closer to a 2% change per degree of global warming.

Another way of expressing the increasing importance of oceanic moisture supply in continental hydrology is through the percentage of continental precipitation originating as oceanic evaporation over the three time

TABLE 1. Continental evaporation (ε_c) and precipitation (ρ_c) recycling ratios (unitless) for 60°S–80°N from two reanalysis datasets for present-day time periods and from ESM2G all-historical experiments and RCP8.5 future experiments. ERA-Interim data cover 1979–2014. MERRA data are for 1979–2012. For ESM2G simulations, there are three ensemble members for each time period; label End 19th C covers 1862–84, label End 20th C covers 1982–2004, and label End 21st C covers 2072–99. The left set of columns shows the fraction of continental evaporation going to continental precipitation; the right set of columns shows the fraction of continental precipitation going to continental evaporation.

	ε_c			ρ_c		
	End 19th C	End 20th C	End 21st C	End 19th C	End 20th C	End 21st C
ERA-Interim	—	0.569	—	—	0.395	—
MERRA	—	0.550	—	—	0.425	—
GFDL-ESM2G	0.560	0.550	0.526	0.381	0.375	0.355
Change from earlier time period	0.010	0.024		0.006	0.020	
Percent change	1.8%	4.4%		1.6%	5.3%	
Percentage change per degree change in global mean temperature	3.2% °C^{-1}	1.7% °C^{-1}		2.9% °C^{-1}	2.0% °C^{-1}	

periods (P_o, shown in Fig. 1), which can be determined by subtracting the continental recycling ratios in Table 1 from 1.0. This percentage increases from 61.9% at the end of the nineteenth century to 62.5% at the end of the twentieth century, and to 64.5% at the end of the twenty-first century. Similarly, the percentage of continental evaporation falling as oceanic precipitation (E_o) increases from 44.0%, to 45.0%, and then to 47.4% over the three time periods (Fig. 1).

5. The hydrologic cycle in a warming world

a. Current theory and understanding

The increasing oceanic contribution to continental hydrology is tied to increases in moisture of oceanic origin within the atmospheric reservoir as near-surface temperatures increase. Theory, observations, and modeling results all show that as global temperatures warm, the mean atmospheric moisture content increases (e.g., Held and Soden 2006; Bosilovich et al. 2005). Coupled with a slower rate of increase of precipitation (~1%–3% K^{-1} for precipitation as compared with the Clausius–Clapeyron rate of 7% K^{-1} for lower tropospheric water vapor; Held and Soden 2006), this leads to the conclusion that the convective mass flux of moisture from the boundary layer to the free troposphere must decrease (Held and Soden 2006) while the atmospheric moisture residence time must increase (Bosilovich et al. 2005). Held and Soden (2006) also show that these increases in lower-tropospheric humidity should lead to proportional increases in the existing global pattern of mean surface $E - P$; consistent with this expectation, observations and modeling studies of sea surface salinity (SSS) found increasing SSS in the evaporation-dominated midlatitudes, suggesting increased net oceanic evaporation, and decreasing salinities in the rainfall-dominated tropical convergence zones (Durack et al. 2012).

Of the hydrologic exchanges quantified in Fig. 1, late-twenty-first-century minus late-twentieth-century increases are seen in total annual evaporative flux from both land and ocean, in total precipitation over both land and ocean, and in water vapor transport to and from the ocean. These results are consistent with current understanding about the hydrologic cycle in a warming world described above. On the other hand, the land-to-land water vapor transport decreases. This likely reflects the increased atmospheric moisture residence time discussed above, as well as the decline in continental moisture recycling ratios described throughout this paper. The decline is tempered by increasing evaporation from land. The zonal mean behavior discussed below indicates that regional processes are more nuanced, with influences from local circulation, local soil moisture availability to meet increased atmospheric evaporative demand, and zonal extent of landmasses. Such regional issues, which may be essential for understanding how future recycling change will affect regional hydroclimate and water budgets, will be explored in detail in follow-up work.

As atmospheric temperatures and evaporative demand increase, near-surface humidity is expected to respond to the unlimited moisture source over oceans and soil moisture limitations on evaporation from land with approximately equal changes in the ratio of future (q_f) to present (q_p) humidity over land and ocean, that is, $(q_f/q_p)_{\text{land}} \approx (q_f/q_p)_{\text{ocean}}$ (e.g., Byrne and O'Gorman 2016; Chadwick et al. 2016). This is equivalent to an atmospheric moisture constraint requiring equal fractional changes in specific humidity over land and ocean, or a time-invariant ratio $\gamma = q_{\text{land}}/q_{\text{ocean}}$. Byrne and O'Gorman (2018) combine this atmospheric moisture constraint with a constraint that the moist static energy or moist enthalpy changes over land and

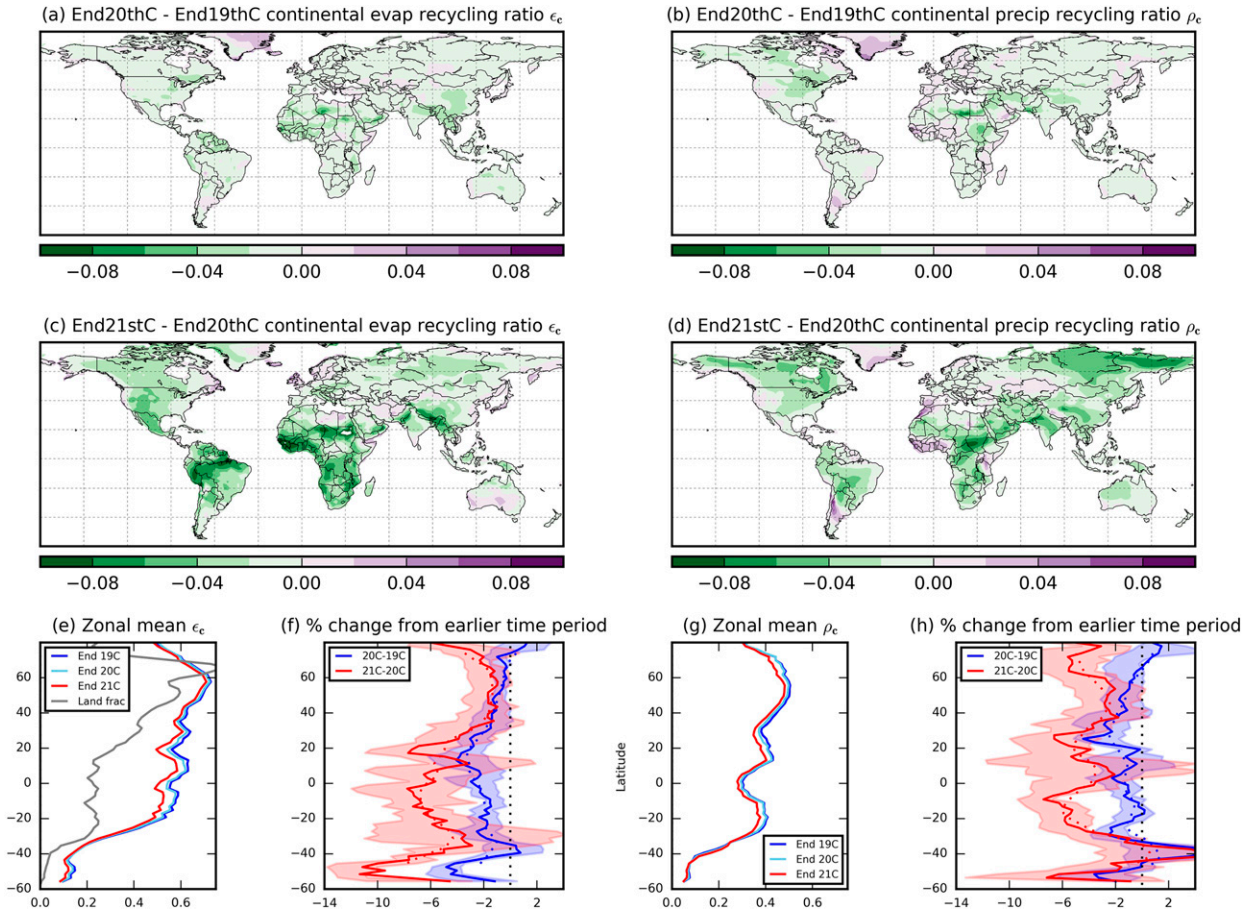

FIG. 3. Differences of average continental (left) evaporation and (right) precipitation recycling ratios (a),(b) between the end of the twentieth and nineteenth centuries and (c),(d) between the end of the twenty-first and twentieth centuries. Also shown are the associated (e),(g) zonal means and (f),(h) zonal mean differences. The shaded areas in (f) and (h) show the 25th–75th percentile ranges of the difference fields across that zonal band. Zonal mean land fraction is also included in (e). South of 20°S, zonal mean ratios decrease rapidly as zonal mean land coverage decreases.

ocean are equal to formulate a simple analytical theory to interpret the differential responses of land and ocean T and q to climate change. Implicit in the theory is the assumption that circulation does not change appreciably between present and future. The ESM2G simulations demonstrate consistency with this theory: throughout the RCP8.5 simulations, γ is constant at 0.65 from 60°S to 80°N or 0.70 from 40°S to 40°N (as compared with 0.72 from ERA-Interim for 40°S to 40°N; Byrne and O'Gorman 2018), and the rate of change of moist enthalpy over both land and ocean holds constant at $0.08\,\mathrm{kJ\,kg^{-1}\,yr^{-1}}$ (see Figs. S1 and S2 in the online supplemental material).

b. *Simple mixing-based prototype model of continental moisture recycling*

Given evidence that the large-scale dynamical conditions are approximately unchanged throughout our simulations, we evaluate the future change in moisture recycling through a simple prototype of an atmospheric moisture column for which oceanic and continental source contributions change differentially. Using this single-column model, we derive an equation for the future precipitation recycling ratio ρ_{cf} as a function of the initial recycling ratio ρ_{ci}, the initial oceanic and continental evaporation rates, and the fractional rates of change of oceanic and continental evaporation [i.e., Eq. (3) derived below].

The simple prototype assumes a rapidly mixed column of moist air with some moisture of oceanic origin, M_o, and some moisture of continental origin, M_c. The continental precipitation recycling ratio ρ_c is given by Eq. (1), where each term represents precipitation tracked backward to an evaporation source. Here the variable M indicates that these moisture terms originate as evaporation from either continental or oceanic regions and subsequently fall as precipitation over land.

We can estimate how changes in evaporation from an initial time to a future time (subscripts i and f) impact the recycling ratio, given changes in continental and oceanic evaporation at fractional rates of r_c and r_o, respectively:

$$\rho_{cf} = \frac{M_{cf}}{M_{cf} + M_{of}} = \frac{M_{ci} + \Delta M_c}{M_{ci} + \Delta M_c + M_{oi} + \Delta M_o} = \frac{M_{ci} + r_c M_{ci}}{M_{ci} + r_c M_{ci} + M_{oi} + r_o M_{oi}} = \frac{(1 + r_c) M_{ci}}{(1 + r_c) M_{ci} + (1 + r_o) M_{oi}}.$$

Here we have assumed that $\Delta M_c = r_c M_{ci}$ and $\Delta M_o = r_o M_{oi}$, that is, that future minus initial differences in column moisture from continental and oceanic sources can be expressed as the product of the initial state moisture contributions from continents and oceans and the fractional rates of change of continental and oceanic evaporation. After manipulation,

$$\rho_{cf} = \rho_{ci} \frac{\left(1 + \frac{\Delta M_c}{M_{ci}}\right)}{\left[1 + \frac{(\Delta M_c + \Delta M_o)}{(M_{ci} + M_{oi})}\right]}. \quad (3)$$

Thus,

$$\rho_{cf} < \rho_{ci} \quad \text{for} \quad \frac{(\Delta M_c + \Delta M_o)}{(M_{ci} + M_{oi})} > \frac{\Delta M_c}{M_{ci}}.$$

Further manipulation shows that this condition holds when $r_o > r_c$. In other words, the continental precipitation recycling ratio must decrease if the rate of increasing oceanic evaporation is larger than the rate of increasing continental evaporation. This condition is likely to hold because continental evaporation is water-limited (e.g., Jung et al. 2010; Zhao and Running 2010). (In high-latitude environments where frozen conditions may become less likely in the future, continental evaporation may increase at faster rates than oceanic evaporation.) Furthermore, this condition can be tested explicitly with evaporation fields from the ESM2G simulations (Fig. 4).

Figure 4c shows that for the region between 50°S and 40°N, zonal mean oceanic evaporation is about 1% higher in the 1990s than the 1870s and is an additional 3%–4% higher in the 2090s. Poleward of 40°N, zonal mean oceanic evaporation increases by more than 15% in the future, with large standard deviations for both time periods driven by highly variable behavior, particularly in the North Atlantic. Changes in continental evaporation rates (Fig. 4b) show broad variability, with the standard deviations of the zonal mean changes including the zero line for the full zonal extent of the difference fields, except for the region north of 40°N for the future. Although the variability is large, the mean red difference curve in Fig. 4b suggests that future continental evaporation will decrease slightly over the subtropics, increase slightly over the tropics, and increase more substantially over the northern midlatitudes.

The prototype model applied here relates changes in continental and oceanic evaporation rates to changes in the continental precipitation recycling ratios. While we should formally interpret r_c and r_o at the global scale, if we assume that zonal moisture transport is fast relative to meridional moisture transport, it is reasonable to consider zonal mean values of r_c and r_o. Additionally, application of the simple prototype to zonal mean behavior helps to bridge the gap between the gridcell-based approach of the full ESM and the highly idealized single-column perspective of the prototype. Figures 4d and 4e show the model's zonal mean r_c and r_o for the twenty-first century for zonal mean values of ρ_c. (Equivalent figures for the twentieth century are shown in Fig. S3 in the online supplemental material.) Changes in zonal mean evaporation rates over both land and oceans are relatively constant for zonal mean present-day ρ_c of less than about 0.3 (Figs. 4d,e). For larger values of ρ_c, the difference between the green and purple dots indicates substantial variability in evaporative changes for zonal bands with similar zonal mean ρ_c, particularly in the approximate range 0.3–0.45. These differences stem from latitudes north of 60°N, indicating the important role of continental geometry. Figure 3g indicates that much of the data between latitudes from 30°S to 70°N have zonal mean values of ρ_c relatively close to 0.4, while the percentage of land area in each of these zonal bands varies between about 20% for much of the tropics, up to about 55% by 40°N, peaking at about 78% just north of 60°N (Fig. 3e). This difference in fractional land area could be an important contributor to the variability in evaporative changes noted above.

Figure 5 shows the impact of changing evaporation rates on the recycling ratios, using ESM2G's zonal mean values in the simple prototype. Figures 5b and 5d highlight the relationship between the reference precipitation recycling ratio ρ_{ci} on the x axis and the normalized change between values from two time periods, that is, $(\rho_{cf} - \rho_{ci})/\rho_{ci}$, for some combinations of r_o and r_c. For each time period, the blue lines are the single-column prototype estimates with constant evaporation increases informed by the range of values coming from the model's zonal mean results shown in Figs. 4b and 4c: ($r_c = 0\%$; $r_o = 5\%$) and ($r_c = -5\%$; $r_o = 10\%$) for the

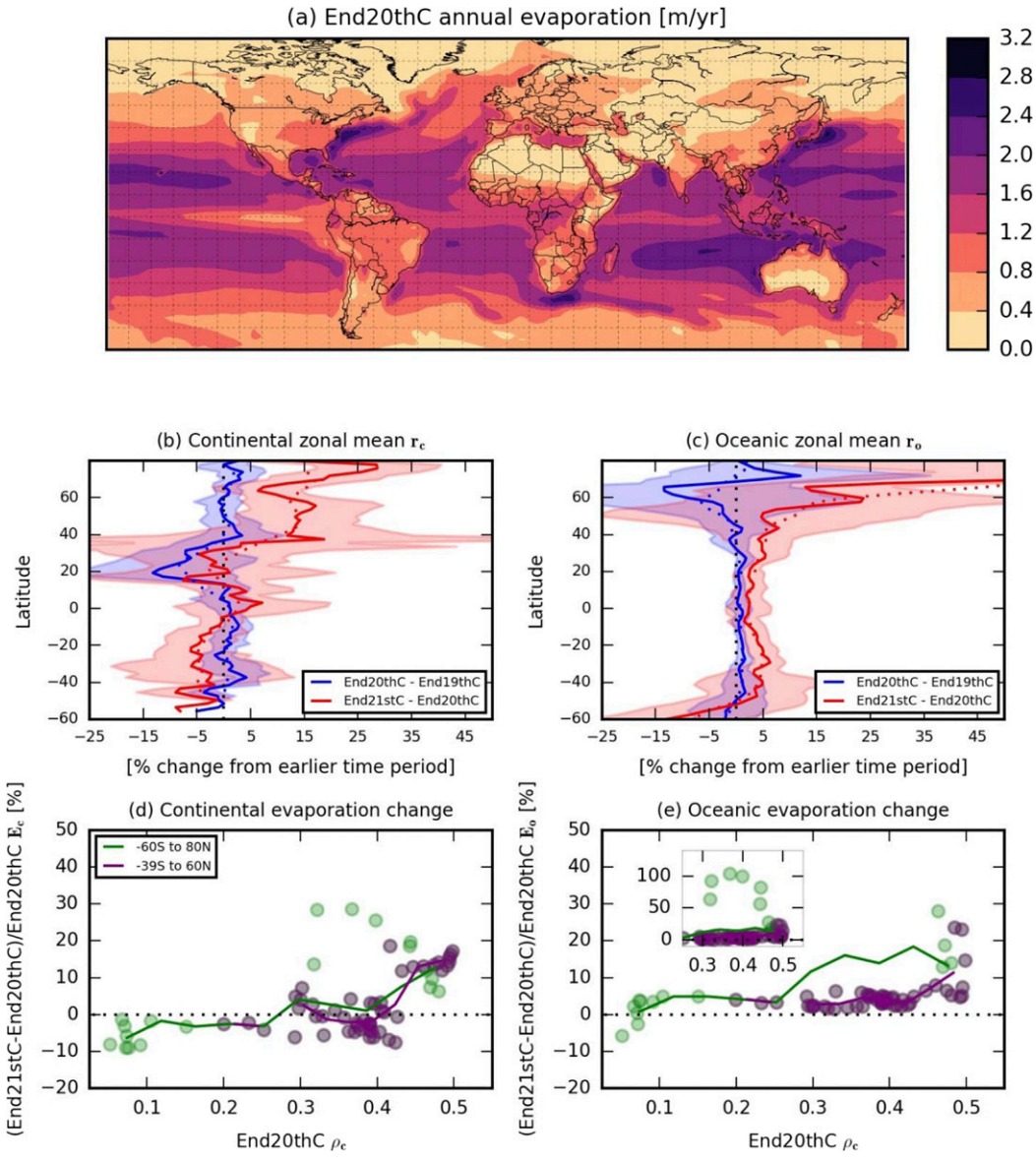

FIG. 4. (a) Annual evaporation for the end of the twentieth century; and percent change in zonal mean (b) continental and (c) oceanic evaporation between the end of the twentieth and nineteenth centuries (blue lines) and the end of the twenty-first and twentieth centuries (red lines). Shaded regions in (b) and (c) are ±1 standard deviation for values across that zonal band. Also shown are zonal mean values of future change in (d) continental and (e) oceanic evaporation [red lines in (b) and (c)] plotted against corresponding continental precipitation recycling ratio from the end of the twentieth century (light blue line in Fig. 3g). Purple dots indicate zonal mean values from 40°S to 60°N, and green dots are for values from 60°S to 80°N. The inset figure in (e) is for very large values from latitudes between 60° and 80°N (note the expanded *y*-axis range on the inset plot).

future, along with (r_c = 0%; r_o = 1%) and (r_c = 0%; r_o = 5%) for the past. The red lines are prototype estimates when the evaporation increase rates are dependent on present-day ρ_c (Figs. 4d and 4e for future minus present; supplemental Figs. S3a and S3b for present minus past). Using these zonal mean values in the prototype demonstrates qualitative consistency between the prototype and the results from ESM2G. This suggests that the prototype captures the broad picture of the changes in precipitation recycling ratios with changing evaporation rates, although spatiotemporal variability and complexities inherent in fully coupled models limit the degree of correspondence to the prototype results.

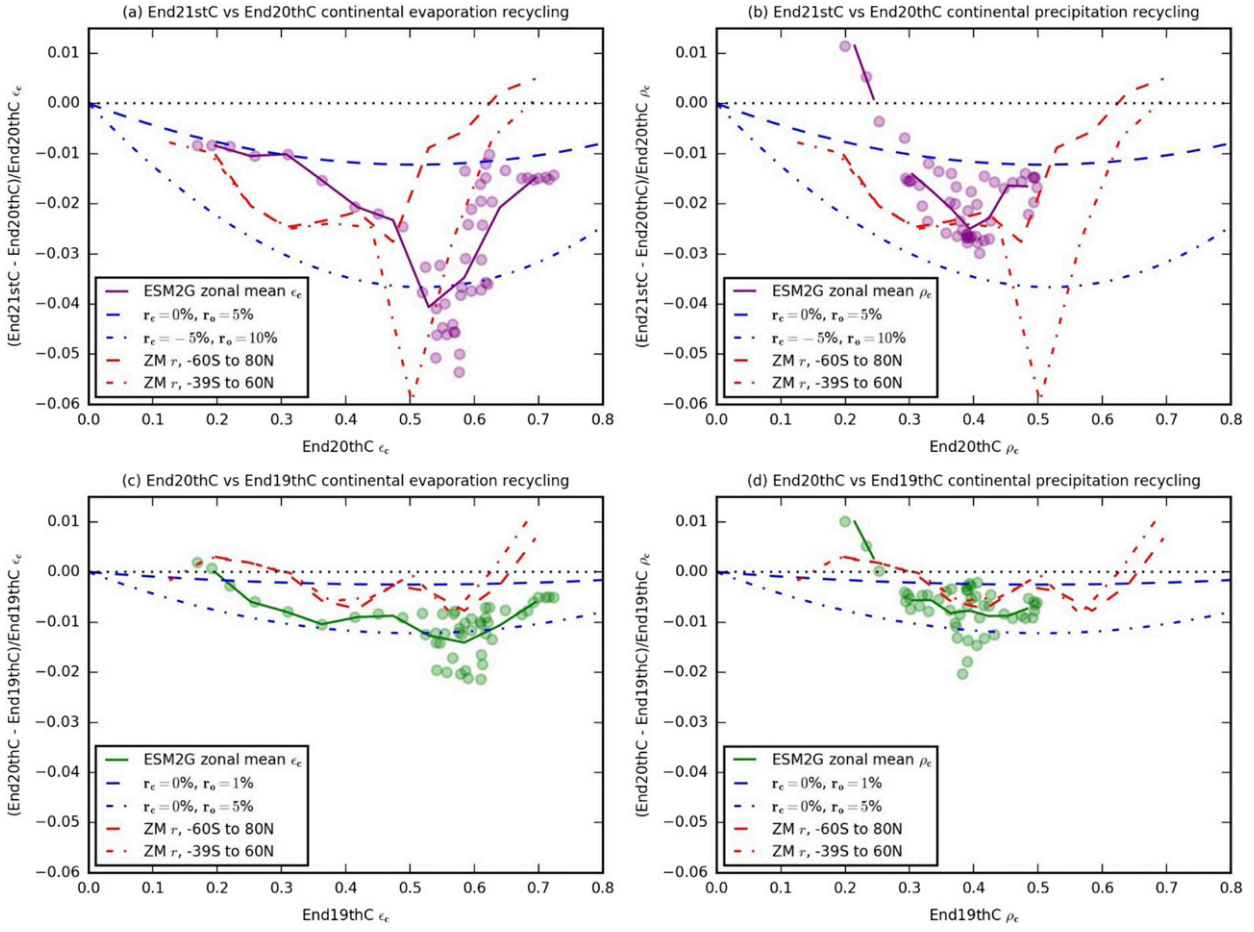

FIG. 5. Zonal mean values of percent change in continental (left) evaporation and (right) precipitation recycling ratios for the (a),(b) twenty-first century minus the twentieth century and (c),(d) twentieth century minus the nineteenth century plotted against corresponding continental recycling ratio from the earlier time period. Blue lines are results from the simple model, given the best estimates of the average rates of continental and oceanic increases in the recycling ratios from Fig. 4, as specified in the legend. Red lines are computed with variable r_o and r_c values from Figs. 4d and 4e for changes in the future in (a) and (b) and from supplementary Fig. S3 for changes from the past in (c) and (d).

Given the assumption of instantaneous mixing, the simple prototype cannot be directly extended to capture changes in the behavior of the continental evaporation recycling ratio since the terms in the ε_c definition [Eq. (2)] reflect a shared terrestrial evaporation source, but different atmospheric residence times and transport distances to terrestrial and oceanic destinations. The impact of increased atmospheric residence times with warming global temperatures (e.g., Held and Soden 2006) on ε_c is being explored for future publication. In Figs. 5a and 5c we compare the model's zonal mean changes in continental evaporation recycling ratio to the prototype estimates for changes in the continental precipitation recycling ratios. These figures demonstrate that changes in ε_c are similar in magnitude to changes in ρ_c and are thus within expectations derived from reasonable estimates of changes in oceanic and terrestrial evaporation rates.

c. *Impact of increased soil moisture availability*

The simple mixing prototype indicates that differences in the rates of change of continental versus oceanic evaporation largely control changes in continental recycling ratios. Water limitation at the land surface is of leading-order importance in continental evaporation. To better understand the impact of continental water limitation, we analyze the GFDL model simulations included in the GLACE-CMIP5 project (Seneviratne et al. 2013; Berg et al. 2016) in which soil moisture overrides alter the availability of soil moisture. Two perturbation experiments are compared with an RCP8.5 control experiment. In Exp1A, interactive soil moisture

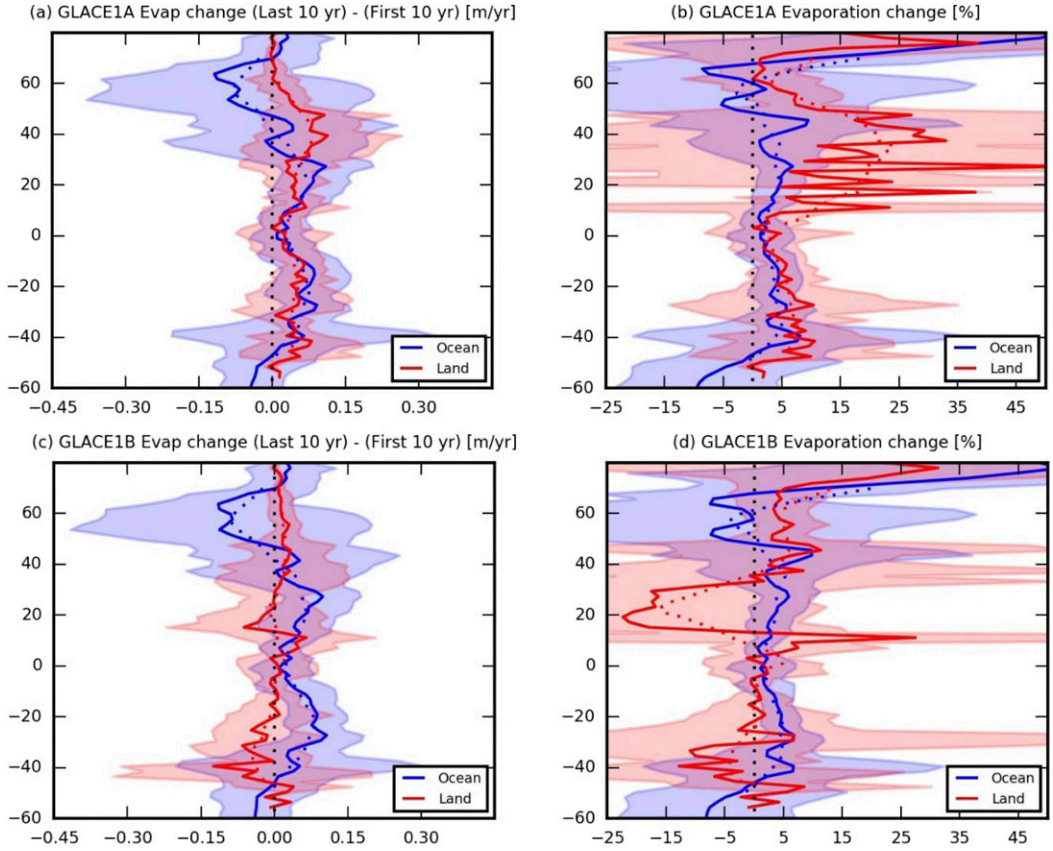

FIG. 6. Changes in evaporation in the (a),(b) GLACE1A and (c),(d) GLACE1B simulations with ESM2M, showing the (left) change in zonal mean evaporation over the ocean (blue) and land (red) between the first and last 10 years [$E_{(2091–2100)} - E_{(2006–2015)}$] and (right) the same thing, but normalized by the value in the first 10 years.

calculated in a RCP8.5-type experiment is replaced with a fixed 30-yr climatology determined from the model years 1971–2000 from historical experiments. In Exp1B, interactive soil moisture is replaced with a 30-yr climatology determined from a 30-yr moving window. Both soil moisture override experiments reduce soil moisture limitation relative to the control experiment by suppressing the occurrence of soil moisture dry spells that typically reduce evaporation (e.g., Berg et al. 2015). However, because the running soil moisture climatology in Exp1B is generally drier over the twenty-first century than in Exp1A, soil moisture limitation remains greater in Exp1B than in Exp1A (Berg et al. 2016). Figure 6 shows zonal mean differences of evaporation between the first 10 years and the last 10 years of these simulations. Given that the availability of soil moisture for land evaporation determines the ratio γ, the reduced soil moisture limitation of both Exp1A and Exp1B (relative to the control RCP8.5 experiment) should lead to larger (but still constant) values of γ. Indeed, for 60°S–80°N, Exp1A and Exp1B have constant values of 0.68 and 0.67, respectively, as compared with the aforementioned $\gamma_{\mathrm{RCP8.5}}$ value of 0.65. For 40°S–40°N, $\gamma_{1A} = 0.74$, $\gamma_{1B} = 0.72$, and $\gamma_{\mathrm{RCP8.5}} = 0.70$. The larger values of γ in the experiments with reduced soil moisture limitation are accompanied by larger r_c rates. In the simple mixing prototype, larger values of r_c with the same r_o in the future yield smaller reductions of the continental precipitation recycling ratio. Thus, oceanic evaporation is not the only controlling factor on continental hydrology, since the availability of soil moisture can temper the influence of both the ocean and the atmosphere (e.g., Berg et al. 2016).

6. Conclusions

Although there is uncertainty in the precise values of the continental moisture recycling ratios (across different reanalysis datasets, different moisture tracking algorithms, and different GCMs or ESMs), the directionality of the impact of increasing greenhouse gases and increasing atmospheric temperatures on this broad measure of the global hydrological cycle is well explained by theory and captured by ESM2G and

WAM-2layers. The consistency among theoretical arguments, the simple mixing prototype, and the WAM-2layers analysis of ESM2G output points to the robustness of our results and suggests that the conclusions are not model-dependent. Overall, we find a systematic reduction in continental precipitation and evaporation recycling ratios in a warming world for which an increasing proportion of atmospheric column moisture originates from oceanic source regions.

These results are captured in Fig. 1, which shows that global precipitation and evaporation are expected to increase over both land and ocean in a warming world, and that in light of moisture limitation over land, the ocean's relative role in the global hydrological cycle increases as global temperatures warm. These findings address a critical component of the GEWEX directive for improved understanding of global hydrologic exchanges in the current and changing climate.

The slight reduction of future terrestrial moisture recycling documented here may be seen as dampening, in a global sense, the potential impacts of future land use change on terrestrial sources of evaporation as global temperatures increase (e.g., Keys et al. 2016). However, continued study is warranted to fully understand how climate change may impact moisture recycling in specific regions. Key sources of terrestrial evaporation, notably the interior of the Amazon basin and parts of the Ganges-Brahamputra and Indus River basins, may experience reductions in moisture recycling (Figs. 3c,d). Likewise, key sinks of terrestrial recycled precipitation, such as the La Plata River basin, the corn producing regions of North America, and parts of East Asia, are worthy of future study, given their critical importance to agricultural production.

Acknowledgments. The authors appreciate helpful input from Nadir Jeevanjee, Salvatore Pascale, and three anonymous reviewers. Author BRL acknowledges support from NSF-AGS-1505198. No authors have competing financial interests.

APPENDIX

Constraints Imposed to Ensure Consistency between Forward and Backward Tracking

Minor numerical losses of water arise from temporal interpolation of WAM-2layers input fields from 3- or 6-hourly data down to 15-min increments, from the vertical interpolation of full atmospheric profiles of wind and humidity down to two layers, and from the neglect of frozen and liquid water in the atmosphere (only water vapor is tracked). For the forward tracking routine, total loss terms ($\mathrm{TotWL_{for}}$) for the ESM2G calculations amount to about 2% of continental evaporation during each analysis time period (Fig. S4b in the online supplemental material). For the backward tracking, losses total ($\mathrm{TotWL_{back}}$) 8%–9% of continental precipitation, concentrated spatially over the leeward edge of mountain chains (supplemental Fig. S4a). Losses are smaller in the WAM-2layers runs with reanalysis products: less than 0.1% in both forward tracking analyses, and 4.3% and 1.7% in the backtracking analyses with ERA-Interim and MERRA, respectively.

These losses lead to an imperfect balance between the forward tracking of continental evaporation until it precipitates out over land (P_c), and the backward tracking of continental precipitation to its source as land-based evaporation (E_c). In the annual mean, these terms should be identical. We apply a correction procedure to account for loss terms and ensure that $P_{c\_\mathrm{corr}} = E_{c\_\mathrm{corr}}$.

First, to account for the water lost during the forward tracking routine, we scale the tracked terms by a global constant equal to 1 plus the loss percentage:

$$P_{c\_\mathrm{corr}} = P_c\left(1 + \frac{\mathrm{TotWL_{for}}}{E_{\mathrm{Land}}}\right).$$

The application of a global correction to the backward tracking losses would be inconsistent with the source regions for the losses coming primarily from mountainous land regions (Fig. S4a in the online supplemental material). Instead, we force the backward tracking losses to be split between the continent and the ocean such that $P_{c\_\mathrm{corr}} = E_{c\_\mathrm{corr}}$:

$$\mathrm{WL_{back,}}_c = P_{c\_\mathrm{corr}} - E_c,$$

$$\mathrm{WL_{back,}}_o = \mathrm{TotWL_{back}} - \mathrm{WL_{back,}}_c, \quad \text{and}$$

$$E_{c\_\mathrm{corr}} = \mathrm{WL_{back,}}_c + E_c.$$

This treatment ensures equivalence between global values determined from the forward tracking and backward tracking presented in the tables and figures in this document. For example, the continental evaporation recycling ratio determined from the backward tracking routine is equal to the fraction of continental evaporation precipitating onto land determined from the forward tracking routine:

$$\varepsilon_c = \frac{E_{c\_\mathrm{corr}}}{E_{\mathrm{Land}}} = \frac{P_{c\_\mathrm{corr}}}{E_{\mathrm{Land}}}.$$

Similarly, the continental precipitation recycling ratio determined from the forward tracking routine is equal to the fraction of continental precipitation derived from

continental sources, as determined from the backward tracking routine:

$$\rho_c = \frac{P_{c\_\mathrm{corr}}}{P_{\mathrm{Land}}} = \frac{E_{c\_\mathrm{corr}}}{P_{\mathrm{Land}}}.$$

Since the loss terms are very similar for each of the three time periods studied, this correction procedure shifts the values of the recycling ratios by the same amount for each time period. Thus, $\Delta\varepsilon_c = \Delta\varepsilon_{c\_\mathrm{corr}}$, where Δ indicates the difference in recycling ratio between time periods. The same is true for the precipitation recycling terms: $\Delta\rho_c = \Delta\rho_{c\_\mathrm{corr}}$.

Table S1 in the online supplemental material provides uncorrected values of both continental recycling ratios for all datasets and time periods discussed in this paper. All other tables, figures, and equations use values after these correction procedures have been applied. Incremental changes in continental moisture recycling ratios are nearly identical in Table 1 and supplemental Table S1, indicating that these changes are unaffected by the correction for numerical water losses in the tracking algorithm.

REFERENCES

Anderson, J. L., and Coauthors, 2004: The new GFDL global atmosphere and land model AM2–LM2: Evaluation with prescribed SST simulations. *J. Climate*, **17**, 4641–4673, https://doi.org/10.1175/JCLI-3223.1.

Berg, A., and Coauthors, 2015: Interannual coupling between summertime surface temperature and precipitation over land: processes and implications for climate change. *J. Climate*, **28**, 1308–1328, https://doi.org/10.1175/JCLI-D-14-00324.1.

——, and Coauthors, 2016: Land–atmosphere feedbacks amplify aridity increase over land under global warming. *Nat. Climate Change*, **6**, 869–874, https://doi.org/10.1038/nclimate3029.

Bosilovich, M. G., and J.-D. Chern, 2006: Simulation of water sources and precipitation recycling for the MacKenzie, Mississippi, and Amazon River basins. *J. Hydrometeor.*, **7**, 312–329, https://doi.org/10.1175/JHM501.1.

——, S. D. Schubert, and G. K. Walker, 2005: Global changes of the water cycle intensity. *J. Climate*, **18**, 1591–1608, https://doi.org/10.1175/JCLI3357.1.

——, F. R. Robertson, and J. Chen, 2011: Global energy and water budgets in MERRA. *J. Climate*, **24**, 5721–5739, https://doi.org/10.1175/2011JCLI4175.1.

Byrne, M. P., and P. A. O'Gorman, 2016: Understanding decreases in land relative humidity with global warming: Conceptual model and GCM simulations. *J. Climate*, **29**, 9045–9061, https://doi.org/10.1175/JCLI-D-16-0351.1.

——, and ——, 2018: Trends in continental temperature and humidity directly linked to ocean warming. *Proc. Natl. Acad. Sci. USA*, **115**, 4863–4868, https://doi.org/10.1073/pnas.1722312115.

Chadwick, R., P. Good, and K. M. Willett, 2016: A simple moisture advection model of specific humidity change over land in response to SST warming. *J. Climate*, **29**, 7613–7632, https://doi.org/10.1175/JCLI-D-16-0241.1.

Dee, D. P., and Coauthors, 2011: The ERA-Interim reanalysis: Configuration and performance of the data assimilation system. *Quart. J. Roy. Meteor. Soc.*, **137**, 553–597, https://doi.org/10.1002/qj.828.

Delworth, T. L., and Coauthors, 2006: GFDL's CM2 global coupled climate models. Part I: Formulation and simulation characteristics. *J. Climate*, **19**, 643–674, https://doi.org/10.1175/JCLI3629.1.

Dirmeyer, P. A., and K. L. Brubaker, 2007: Characterization of the global hydrologic cycle from a back-trajectory analysis of atmospheric water vapor. *J. Hydrometeor.*, **8**, 20–37, https://doi.org/10.1175/JHM557.1.

——, J. Wei, M. G. Bosilovich, and D. M. Mocko, 2014: Comparing evaporative sources of terrestrial precipitation and their extremes in MERRA using relative entropy. *J. Hydrometeor.*, **15**, 102–116, https://doi.org/10.1175/JHM-D-13-053.1.

Dominguez, F., P. Kumar, X.-Z. Liang, and M. Ting, 2006: Impact of atmospheric moisture storage on precipitation recycling. *J. Climate*, **19**, 1513–1530, https://doi.org/10.1175/JCLI3691.1.

Dunne, J. P., and Coauthors, 2012: GFDL's ESM2 global coupled climate–carbon Earth system models. Part I: Physical formulation and baseline simulation characteristics. *J. Climate*, **25**, 6646–6665, https://doi.org/10.1175/JCLI-D-11-00560.1.

——, and Coauthors, 2013: GFDL's ESM2 global coupled climate–carbon Earth system models. Part II: Carbon system formulation and baseline simulation characteristics. *J. Climate*, **26**, 2247–2267, https://doi.org/10.1175/JCLI-D-12-00150.1.

Durack, P. J., S. E. Wijffels, and R. J. Matear, 2012: Salinities reveal strong water cycle intensification during 1950 to 2000. *Science*, **336**, 455–458, https://doi.org/10.1126/science.1212222.

Hallberg, R., and A. Adcroft, 2009: Reconciling estimates of the free surface height in Lagrangian vertical coordinate ocean models with mode-split time stepping. *Ocean Modell.*, **29**, 15–26, https://doi.org/10.1016/j.ocemod.2009.02.008.

Held, I. M., and B. J. Soden, 2006: Robust responses of the hydrological cycle to global warming. *J. Climate*, **19**, 5686–5699, https://doi.org/10.1175/JCLI3990.1.

Jung, M., and Coauthors, 2010: Recent decline in the global land evapotranspiration trend due to limited moisture supply. *Nature*, **467**, 951–954, https://doi.org/10.1038/nature09396.

Keys, P. W., R. J. van der Ent, L. J. Gordon, H. Hoff, R. Nikoli, and H. H. G. Savenije, 2012: Analyzing precipitationsheds to understand the vulnerability of rainfall dependent regions. *Biogeosciences*, **9**, 733–746, https://doi.org/10.5194/bg-9-733-2012.

——, E. A. Barnes, R. J. van der Ent, and L. J. Gordon, 2014: Variability of moisture recycling using a precipitationshed framework. *Hydrol. Earth Syst. Sci.*, **18**, 3937–3950, https://doi.org/10.5194/hess-18-3937-2014.

——, L. Wang-Erlandsson, and L. J. Gordon, 2016: Revealing invisible water: Moisture recycling as an ecosystem service. *PLOS* ONE, **11**, e0151993, https://doi.org/10.1371/JOURNAL.PONE.0151993.

Koster, R. D., and Coauthors, 1986: Global sources of local precipitation as determined by the NASA/GISS GCM. *Geophys. Res. Lett.*, **13**, 121–124, https://doi.org/10.1029/GL013i002p00121.

Lorenz, C., and H. Kunstmann, 2012: The hydrological cycle in three state-of-the-art reanalyses: Intercomparison and performance analysis. *J. Hydrometeor.*, **13**, 1397–1420, https://doi.org/10.1175/JHM-D-11-088.1.

Seneviratne, S. I., and Coauthors, 2013: Impact of soil moisture-climate feedbacks on CMIP5 projections: First results from the GLACE-CMIP5 experiment. *Geophys. Res. Lett.*, **40**, 5212–5217, https://doi.org/10.1002/grl.50956.

Shevliakova, E., and Coauthors, 2009. Carbon cycling under 300 years of land use change: importance of the secondary vegetation sink. *Global Biogeochem. Cycles*, **23**, GB2022, https://doi.org/10.1029/2007GB003176.

Soden, B. J., and I. M. Held, 2006: An assessment of climate feedbacks in coupled ocean–atmosphere models. *J. Climate*, **19**, 3354–3360, https://doi.org/10.1175/JCLI3799.1.

Taylor, K. E., R. J. Stouffer, and G. A. Meehl, 2012: An overview of CMIP5 and the experiment design. *Bull. Amer. Meteor. Soc.*, **93**, 485–498, https://doi.org/10.1175/BAMS-D-11-00094.1.

Trenberth, K. E., 1999: Atmospheric moisture recycling: Role of advection and local evaporation. *J. Climate*, **12**, 1368–1381, https://doi.org/10.1175/1520-0442(1999)012<1368:AMRROA>2.0.CO;2.

——, J. T. Fasullo, and J. Mackaro, 2011: Atmospheric moisture transports from ocean to land and global energy flows in reanalyses. *J. Climate*, **24**, 4907–4924, https://doi.org/10.1175/2011JCLI4171.1.

van der Ent, R. J., H. H. G. Savenije, B. Schaefli, and S. Steele-Dunne, 2010: Origin and fate of atmospheric moisture over continents. *Water Resour. Res.*, **46**, W09525, https://doi.org/10.1029/2010WR009127.

——, O. A. Tuinenburg, H.-R. Knoche, H. Kuntsmann, and H. H. G. Savenije, 2013: Should we use a simple or complex model for moisture recycling and atmospheric moisture tracking? *Hydrol. Earth Syst. Sci.*, **17**, 4869–4884, https://doi.org/10.5194/hess-17-4869-2013.

——, L. Wang-Erlandsson, P. W. Keys, and H. H. G. Savenije, 2014: Contrasting roles of interception and transpiration in the hydrological cycle—Part 2: Moisture recycling. *Earth Syst. Dyn.*, **5**, 471–489, https://doi.org/10.5194/esd-5-471-2014.

Winton, M., 2000: A reformulated three-layer sea ice model. *J. Atmos. Oceanic Technol.*, **17**, 525–531, https://doi.org/10.1175/1520-0426(2000)017<0525:ARTLSI>2.0.CO;2.

Zhao, M., and S. W. Running, 2010: Drought-induced reduction in global terrestrial net primary production from 2000 through 2009. *Science*, **329**, 940–943, https://doi.org/10.1126/science.1192666.